Electrostatic solitary structures associated with the November 10, 2003, interplanetary shock at 8.7 AU

J. D. Williams,[1] L.-J. Chen,[1] W. S. Kurth,[1] D. A. Gurnett,[1] M. K. Dougherty,[2] and A. M. Rymer[3]

Received 5 April 2005; revised 22 July 2005; accepted 9 August 2005; published 7 September 2005.

[1] We document the presence of solitary structures in the electric field, measured by the Cassini plasma wave instrument at an interplanetary shock associated with the October/November 2003 solar flares. The occurrence frequency of electrostatic solitary waves increases prior to and during the passage of the initial shock boundary but decreases to almost zero in the post-shock environment. The electric field amplitudes of the solitary structures are on the order of a few tens of μV/m, while the characteristic scale size is estimated to be ∼500 Debye lengths. The estimated potentials are ∼0.5 V both upstream and downstream of the shock. These measurements present a new plasma regime which support electrostatic solitary structures. **Citation:** Williams, J. D., L.-J. Chen, W. S. Kurth, D. A. Gurnett, M. K. Dougherty, and A. M. Rymer (2005), Electrostatic solitary structures associated with the November 10, 2003, interplanetary shock at 8.7 AU, *Geophys. Res. Lett.*, *32*, L17103, doi:10.1029/2005GL023079.

1. Introduction

[2] The October/November 2003 solar disturbance produced five solar flares with intensities greater than X5. The coronal mass ejections associated with these flares traveled out from the Sun and generated interplanetary shocks ahead of them. On November 10, 2003, the Cassini spacecraft, at 8.7 AU, measured plasma waves both before and after the passage of an interplanetary shock. To the best of our knowledge, there has been no report on solitary waves observed at interplanetary shocks. In this letter we describe observations of electrostatic solitary structures associated with the shock passage and compare to observations of solitary waves near Earth's bow shock and in the unshocked solar wind.

[3] Electrostatic structures have been observed in different space environments, including the magnetotail [*Matsumoto et al.*, 1994], the auroral region [*Ergun et al.*, 1998], the magnetosheath [*Pickett et al.*, 2005, and references therein], and the solar wind [*Mangeney et al.*, 1999]. Of particular interest to our study are the observations of solitary structures in the bow shock transition region by *Bale et al.* [1998, 2002] and in association with Sudden Large Amplitude Magnetic Structures (SLAMS) upstream of the Earth's bow shock by *Behlke et al.* [2004]. *Bale et al.* [2002] have shown for 33 separate bow shock crossings that the majority of solitary structures are observed at the ramp and overshoot portion of the shock and to a lesser extent in the undershoot and downstream regions. *Bale et al.* [1998] suggested that the solitary structures propagated with the solar wind and from that determined the potential structure scale size to range between 2–7 Debye lengths, (λ_D). *Behlke et al.* [2004] determined the scale size of the negative potential structures to be $\sim 10\lambda_D$.

[4] The data are from the Radio and Plasma Wave Science (RPWS) instrument [*Gurnett et al.*, 2004] and the Dual Technique Magnetometer (MAG) [*Dougherty et al.*, 2004] on the Cassini spacecraft. Simultaneous plasma measurements made by the Cassini Plasma Spectrometer (CAPS) are not available. Waveform data from two separate receivers on RPWS are used, they are the wideband receiver (WBR), which measures one component of the electric field and the waveform receiver (WFR), which measures two electric field components and the full vector magnetic field. Important characteristics of WBR are a spectral range of 0.06–10.5 kHz with a resolution of 13.6 Hz and a sample rate of 27,777 samples per second. Likewise, WFR has a spectral range of 0.003–2.5 kHz, a resolution of 3.5 Hz and a sample rate of 7143 samples per second. The solitary wave data presented here came exclusively from the dipole antenna which takes the differential voltage of two cylindrical orthogonal monopoles (each 10m in length). The electric field is determined by dividing the differential voltage measurement by the effective length of the antenna, which is given by the distance between the midpoints of the two monopoles. These monopoles align parallel to the spacecraft X axis, and are symmetric with respect to the spacecraft Z axis which pointed to the Sun during the reported period.

[5] The majority of the measurements presented here are from WBR, which had a 3% duty cycle during the time of the observations; which is a factor of 10 higher than the duty cycle of the WFR instrument. The WBR mode does not provide concurrent magnetic field measurements so we are unable to determine if the electric field disturbances are electrostatic. Complimentary measurements from WFR however, show that those waveforms are electrostatic and so by extension we assume that the solitary waves from WBR are also electrostatic.

2. Observations

[6] We present in Figure 1 an electric field wave power spectrogram for days 314 (November 10) through 318 (November 14) of the year 2003. The shock passage occurs on day 314, at 18:50 UT as evidenced by the broadband

[1]Department of Physics and Astronomy, University of Iowa, Iowa City, Iowa, USA.
[2]Department of Physics, Imperial College, London, UK.
[3]Mullard Space Science Laboratory, University College, London, UK.

0094-8276/05/2005GL023079$05.00

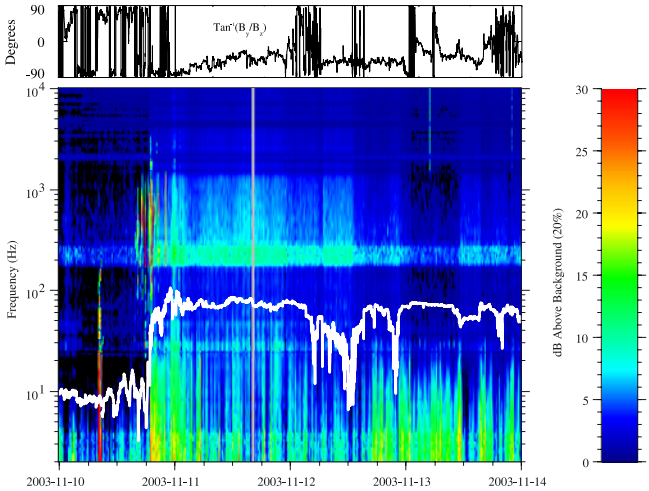

Figure 1. Electric field power as a function of time and frequency. Included on the spectrogram is the electron cyclotron frequency. (top) The magnetic field rotation.

increase in power at that time. The electron cyclotron frequency is overlaid onto the plot and used as a proxy for the magnetic field. At 18:50 UT, the magnetic field changes from 0.4 nT to 1.4 nT, and keeps rising until ~23 UT reaching a maximum of 3.8 nT. The magnetic field stays elevated for approximately 14 days before returning to the pre-shock levels. The brief broadband low-frequency interference near 08:15 on day 314 is due to thruster noise during a reaction wheel biasing activity. The narrow band at 200–300 Hz is also instrumental. The increase in the level of the diffuse background above 0.3 kHz at the time of the shock passage is thought to be an increase in the quasi-thermal noise background, indicative of an increase in plasma density downstream of the shock.

[7] Figure 1 (top) shows the rotation angle of the magnetic field as determined by the arctangent of the ratio of the spacecraft y-component ($\hat{y}_{sc}$ is parallel to $\hat{z}$ of GSE coordinate system) of the magnetic field divided by the spacecraft z-component ($\hat{z}_{sc}$ points radially outward from the Sun) of the magnetic field. The field rotation begins ~5 hours after the shock arrival, indicative of the start of a magnetic cloud [*Burlaga*, 1991], and continues for approximately 30 hours. This situation is roughly analogous to that found at the Earth. First the shock (bow shock), followed by the sheath (magnetosheath), followed by the magnetic cloud (magnetosphere).

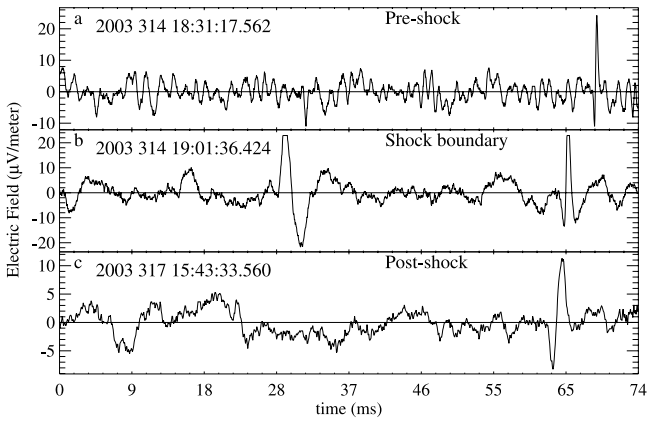

Figure 2. Examples of solitary pulses observed (a) upstream of the shock, (b) during the shock passage itself and (c) downstream of the shock.

[8] The observations presented here are divided into three separate time periods, the 7 hours before the shock arrival called the pre-shock, the 1.5 hours after shock arrival called the shock boundary and the post-shock period. Examples of electrostatic solitary pulses seen during the pre-shock, shock boundary and post-shock periods are shown in Figures 2a, 2b, and 2c, respectively. The ordinate is in milliseconds after the initial time shown in the upper panel of each plot. The abscissa is given in μV/m. Figure 2a shows a bipolar pulse observed approximately 20 minutes before the shock arrival. In Figure 2b, a bipolar pulse is observed at the shock boundary. Figure 2c shows a bipolar structure on day 317. Note that the amplitude of the electric field is in the tens of μV/m range and that it does not change appreciatively over the period of observation. Part of the solitary wave selection criteria are that all pulses must be temporally isolated and must also have large enough amplitudes to be visually seen from among all of the other wave activity. The second structure seen in Figure 2b was not counted because it failed the isolation criteria.

[9] Figure 2a shows the solitary structure embedded within a series of quasi-sinusoidal oscillations. About 30% of the solitary structures were observed to be embedded in some type of quasi-sinusoidal waves, possibly ion acoustic waves as they have a similar timescale to those observed in the solar wind [*Gurnett et al.*, 1979]. The observation may indicate that the ion-acoustic waves are linked to the production of these solitary structures.

[10] To obtain an understanding of when the solitary pulses occur with respect to the shock passage, as well as to show amplitude and time duration variability, we show in Figure 3 the solitary wave events from day 314 to day 328,

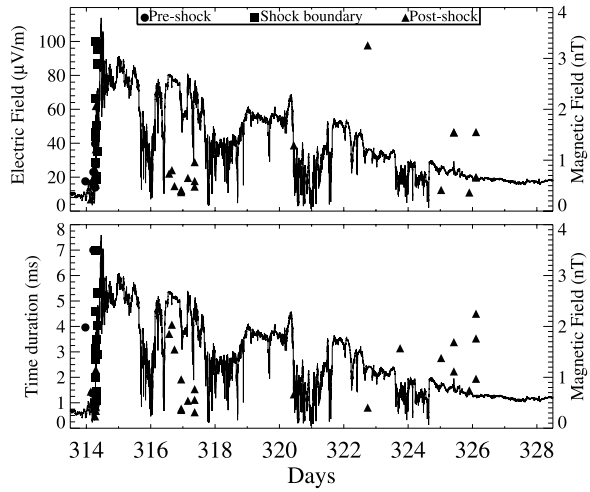

Figure 3. Solitary structures observed from the Oct./Nov. 2003 solar flare events. (top) The peak-to-peak electric field amplitude as a function of time. (bottom) The solitary structure time duration as a function of time. The magnetic field is overlaid onto each panel to give reference to the shock.

overplotted with the ambient magnetic field. Figure 3 (top) shows the pulse peak-to-peak amplitude as a function of time and Figure 3 (bottom) shows the pulse time duration as a function of time. In Figures 3 (top) and 3 (bottom) circles, squares and triangles indicate pre-shock, shock boundary and post-shock pulses, respectively.

[11] A total of 10 solitary structures were detected in the pre-shock region. These are likely to be related to shock-accelerated particles running ahead of the shock. In the shock boundary region another 19 solitary structures were detected. The remaining 20 solitary structures were detected over the course of the next 14 days. The actual times when WBR and WFR data are being taken vary during this 14 day interval. During day 314, data were taken for 2 minute periods at 15 minute intervals. During days 315 to 322 data were taken during 7 minute periods once every hour. From days 322 to 328 data were again taken on the day 314 schedule. This data taking scheme leaves open the possibility that events may be missed. Note that during the 30 hours of the magnetic field rotation shown in Figure 1, no solitary waves are observed although data were taken regularly.

[12] Figure 3 (top) shows that as the magnetic field undergoes the largest change, the electric field amplitude also reaches its peak value. The average peak-to-peak electric field amplitude for the pre-shock environment was determined to be 22.9 ± 8.0 μV/m, the average peak-to-peak amplitude for the shock boundary was 51.1 ± 25.2 μV/m and the post-shock environment amplitude was 29.1 ± 21.6 μV/m. In summary, the average electric field amplitude has no statistically significant change throughout the entire observation period.

[13] Figure 3 (bottom) shows the pulse time durations. These time durations are determined by taking the difference in time between when the pulse rises above and falls below one standard deviation of the mean of the sample. The average time duration for the pre-shock, shock boundary and post-shock environments are 2.5 ± 1.8 ms, 3.2 ± 1.6 ms and 2.4 ± 1.4 ms, respectively. Like the amplitudes, these time durations are statistically the same.

3. Discussion

[14] Our results show that the observation of solitary structures near the shock boundary region, the time span with the largest change in the magnetic field and number density, had the highest occurrence rate of any of the different regions. In the 30 hours of the magnetic field rotation, no solitary structures were observed. From day 317 onward, few solitary waves were observed. Similarly, near Earth, solitary waves are observed preferentially in the shock and sheath regions.

[15] One feature of our observations is that the plasma parameters are quite different from those in which previous solitary structures have been observed, particularly, the electron number density n_e and the magnetic field strength, B ~ 0.4 nT. In order to estimate the number density we use the Langmuir wave frequencies seen in this region of space by RPWS and obtain $n_e \sim 0.07$ cm^{-3}. Such n_e and B values yield a ratio of the gyrofrequency to the plasma frequency, $f_{ce}/f_{pe} \sim 0.004$. This is three orders of magnitude smaller than the $f_{ce}/f_{pe} \sim 5-15$ observed in the auroral region by the FAST satellite [*Ergun et al.*, 1998], and is smaller than those sampled by Polar ($f_{ce}/f_{pe} \sim 0.04-0.4$) [*Franz et al.*, 2000] and in the distant plasma sheet by Geotail ($f_{ce}/f_{pe} \sim 0.06$) [*Matsumoto et al.*, 1994].

[16] The time duration of the pulses as shown in Figure 3 is ~2 ms. In order to see how this time length may translate to the width of the potential structures we use a simple model to relate the speed of the structures to the width:

$$x = \alpha v_s \triangle t,$$

where x is the width of the structure, α is the cosine of the angle the structure takes as it passes over the electric field booms, v_s is the velocity and t is the measured time duration of the structure.

[17] Since the WBR mode only returns the voltage difference of a 1-D dipole antenna we are unable to determine the velocity of the structures. Of the three variables given above only t is known. Due to the small number of data points available, we are unable to estimate the scale size using a Doppler shift analysis [*Mangeney et al.*, 1999]. Histograms of the occurrence probability as a function of the cosine of the angle between the antenna and the magnetic field (not shown) reveal no preferred alignment of the electric field wave vector with the magnetic field. Given the lack of preference of polarization along B and our inability to determine the structure velocity, we assume that the structures travel in the radial solar wind direction. The orientation of the E_x electric field antenna is within 85.5° of the radial solar wind resulting in an $\alpha \cong 0.06$.

[18] In order to estimate the velocity for the solitary structures arriving before the shock we assume that they are produced by particles reflected off the shock which excite solitary waves through a two-stream instability. *Omura et al.* [1996] have shown that solitary structures produced by a two-stream instability will travel at a velocity that is roughly the average of the initial streaming velocities of the two beams. *Hamilton et al.* [2004] estimated the solar wind velocity at Cassini for this interplanetary shock to range between 750–800 km/s based on the pickup ion cutoff. Using 800 km/s as a lower limit of the velocity of one of the streams and a typical solar wind velocity of 400 km/s for the second stream we arrive at v_s = 600 km/s. For the solitary structures detected at or after the shock boundary, we use 800 km/s for the structure velocity.

[19] Using the above values we obtain lower bounds to the scale sizes of $x \sim 20$ km for the pre-shock and $x \sim 27$ km for the post-shock observations. These lead to potential estimates of $\phi \sim 0.4$V (E ~ 20 μV/m) for the pre-shock potential structures and $\phi \sim 0.3$V (E ~ 10 μV/m) for the post-shock potential structures. We are unable to determine the Debye length from the CAPS data, however, using an electron number density ~0.07 cm^{-3} and electron temperature measurements made upstream of Saturn's bow shock ($T_e \sim 3$ eV) by CAPS for the pre-shock plasma environment we estimate $\lambda_D \sim 40$ m for the pre-shock region. Thus, we write the scale size as $x \sim 500\lambda_D$. In the downstream environment we increase the electron number density by a factor of 4, assuming a strong shock [*Gurnett and Bhattacharjee*, 2005], and use the observed changes in T_e from an interplanetary shock observed by CAPS at 5 AU, (T_e increases by a factor of 7) to obtain $\lambda_D \sim 50$ m and $x \sim 500\lambda_D$. Comparing these values to those given by

Bale et al. [1998] ($x \sim 2-7\lambda_D$) and *Behlke et al.* [2004] ($x \sim 10\lambda_D$) we find the scale sizes for the interplanetary shock to be much larger than those for the Earth's bow shock, and in the solar wind at the L1 Lagrange point [*Mangeney et al.*, 1999] ($x \sim 25\lambda_D$).

[20] Even though the structure velocity changes by a factor of approximately 1.5 and the magnetic field increases by a factor of 3.5 our observations indicate that the average time duration of the pulses before and after the shock arrival are the same ($t \sim 2$ ms). These results are similar to results seen in Earth's bow shock by the Cluster mission (J. Pickett, private communication). In comparison, solitary structures in the Earth's bow shock transition region [*Bale et al.*, 1998] ($n_e \sim 45$ per cc, B $\sim$ 10 nT) had a time duration of 0.1 ms, solitary structures observed in the upstream region in association of SLAMS at a quasi-parallel bow shock [*Behlke et al.*, 2004] ($n_e \sim 4$ per cc, B $\sim$ 10 nT) had a time duration of 1 ms, and solitary structures observed in the solar wind at the L1 lagrange point had a time duration 0.3–1 ms [*Mangeney et al.*, 1999].

[21] Under the assumption that the observed solitary structures move in the direction of the radial solar wind, we determine the sign of the potential "hump" as follows. Bipolar structures which first deflect upward and then downward are caused by a positive potential pulse traveling with the solar wind. The opposite case, where first the electric field deflects downward and then upward are caused by a negative potential "hump" traveling with the solar wind. Figure 2a shows a negative potential structure while Figure 2b shows a positive potential structure. Positive potential structures are consistent with electron phase space holes and negative potential structures are consistent with ion phase space holes [*Schamel*, 1986]. Thus, both ion and electron holes are present in our observations. In particular, the observations in Figure 2a indicate an ion hole embedded in ion acoustic-like waves. This is consistent with ion-hole generation by ion acoustic fluctuations observed in a laboratory experiment [*Chan et al.*, 1984].

[22] *Chen et al.* [2004] stated that a solitary structure can be maintained if the gyroradius is much smaller than the scale size of the solitary potential structures. The electron gyroradius, r_e, for this event was calculated from the ratio of the electron thermal velocity to f_{ce}. For the pre-shock environment $r_e = 9$ km and for the post-shock environment $r_e = 3$ km. Comparing the scale sizes calculated above ($x \sim$ 20 km, pre-shock, $x \sim 27$ km, post-shock) to the gyroradii estimates show that for both the upstream and downstream regions the condition was satisfied. This condition is not satisfied for the ion gyroradius, r_i. For the pre-shock environment r_i = 400 km and for the post-shock r_i = 140 km. Thus, for electron holes the ratio of the gyroradius to the scale size may be a relevant consideration of structure stability but new theories must be developed to account for the stability of ion phase space holes.

[23] Solitary structures were observed at 8.7 AU in association with the interplanetary shock generated by the October/November 2003 solar flares. The observations are the first ever observed in such low magnetic field strengths and number densities. The structures themselves were caused by both positive and negative potentials passing over the spacecraft. The characteristic time lengths and amplitudes of the structures changed little with respect to pre- and post-shock plasma environments. Comparison of these results to observations of solitary waves in the Earth's bow shock indicate that the scale sizes are larger for these interplanetary events but that they also occurred in the shock boundary region.

[24] **Acknowledgment.** The research was supported by NSF ATM 03-27540 and by NASA through contract 961152 with the JPL.

References

Bale, S. D., P. J. Kellogg, D. E. Larson, R. P. Lin, K. Goetz, and R. P. Lepping (1998), Biploar electrostatic structures in the shock transition region: Evidence of electron phase space holes, *Geophys. Res. Lett.*, *25*, 2929–2932.

Bale, S. D., A. Hull, D. E. Larson, R. P. Lin, L. Muschietti, P. J. Kellogg, K. Goetz, and S. J. Monson (2002), Electrostatic turbulence and debye-scale structures associated with electron thermalization at collisionless shocks, *Astrophys. J. Lett.*, *575*, L25–L28.

Behlke, R., M. André, S. D. Bale, J. S. Pickett, C. A. Cattell, E. A. Lucek, and A. Balogh (2004), Solitary structures associated with short large-amplitude magnetic structures (SLAMS) upstream of the Earth's quasi-parallel bow shock, *Geophys. Res. Lett.*, *31*, L16805, doi:10.1029/2004GL019524.

Burlaga, L. R. E. (1991), Magnetic clouds, in *Physics of the Inner Heliosphere*, vol. 21, edited by M. C. E. Huber, L. J. Lanzerotti, and D. Stoeffler, pp. 1–19, Springer, New York.

Chan, C., M. H. Cho, N. Hershkowitz, and T. Intrator (1984), Laboratory evidence for ion-acoustic-type double layers, *Phys. Rev. Lett.*, *52*, 1782–1785.

Chen, L.-J., D. J. Thouless, and J.-M. Tang (2004), Bernstein-Greene-Kruskal solitary waves in three-dimensional magnetized plasma, *Phys. Rev. E*, *69*, 055401(R), doi:10.1103/PhysRevE.69.055401.

Dougherty, M. K., et al. (2004), The Cassini magnetic field investigation, *Space Sci. Rev.*, *114*, 331–383, doi:10.1007/s11214-004-1432-2.

Ergun, R. E., C. W. Carlson, J. P. McFadden, F. S. Mozer, L. Muschietti, and I. Roth (1998), Debye-scale plasma structures associated with magnetic-field-aligned electric fields, *Phys. Rev. Lett.*, *81*, 826–829.

Franz, J., P. Kintner, and J. Pickett (2000), On the perpendicular scale size of electron phase space holes, *Geophys. Res. Lett.*, *27*, 169–172.

Gurnett, D. A., and A. Bhattacharjee (2005), *Introduction to Plasma Physics With Space and Laboratory Applications*, 1st ed., Cambridge Univ. Press, New York.

Gurnett, D. A., E. Marsch, W. Pilipp, R. Schwenn, and H. Rosenbauer (1979), Ion acoustic waves and related plasma observations in the solar wind, *J. Geophys. Res.*, *84*, 2029–2038.

Gurnett, D. A., et al. (2004), The Cassini radio and plasma wave investigation, *Space Sci. Rev.*, *114*, 395–463, doi:10.1007/s11214-004-1435-z.

Hamilton, D. C., N. Krupp, D. G. Mitchell, and S. M. Krimigis (2004), Shock events at Cassini associated with the October–November 2003 solar flares, *Eos Trans. AGU*, *85*(17), Jt. Assem. Suppl., Abstract SH32A-05.

Mangeney, A., et al. (1999), Wind observations of coherent electrostatic waves in the solar wind, *Ann. Geophys.*, *17*, 307–320.

Matsumoto, H., H. Kojiima, T. Miyatake, Y. Omura, M. Okada, I. Nagano, and M. Tsutsui (1994), Electrostatic solitary waves (ESW) in the magnetotail: BEN wave forms observed by GEOTAIL, *Geophys. Res. Lett.*, *21*, 2915–2918.

Omura, Y., H. Kojima, and H. Matsumoto (1996), Electron beam instabilities as the generation mechanism of electrostatic solitary waves in the mangetotail, *J. Geophys. Res.*, *101*, 2685–2697.

Pickett, J. S., et al. (2005), On the generation of solitary waves observed by Cluster in the near-Earth magnetosheath, *Nonlinear. Processes Geophys.*, *12*, 181–193.

Schamel, H. (1986), Electron holes, ion holes and double layers electrostatic phase space structures in theory and experiment, *Phys. Rev. E*, *140*, 161–191.

L.-J. Chen, D. A. Gurnett, W. S. Kurth, and J. D. Williams, Department of Physics and Astronomy, University of Iowa, Iowa City, IA 52242, USA. (john-williams@uiowa.edu)

M. K. Dougherty, Department of Physics, Imperial College, London SW7 2BZ, UK.

A. M. Rymer, Mullard Space Science Laboratory, University College, London RH5 6NT, UK.